ENGINEERING

Printing of wirelessly rechargeable solid-state supercapacitors for soft, smart contact lenses with continuous operations

Jihun Park[1,2]*, David B. Ahn[3]*, Joohee Kim[1,2]*, Eunkyung Cha[1,2], Byeong-Soo Bae[4], Sang-Young Lee[3]†, Jang-Ung Park[1,2]†

Recent advances in smart contact lenses are essential to the realization of medical applications and vision imaging for augmented reality through wireless communication systems. However, previous research on smart contact lenses has been driven by a wired system or wireless power transfer with temporal and spatial restrictions, which can limit their continuous use and require energy storage devices. Also, the rigidity, heat, and large sizes of conventional batteries are not suitable for the soft, smart contact lens. Here, we describe a human pilot trial of a soft, smart contact lens with a wirelessly rechargeable, solid-state supercapacitor for continuous operation. After printing the supercapacitor, all device components (antenna, rectifier, and light-emitting diode) are fully integrated with stretchable structures for this soft lens without obstructing vision. The good reliability against thermal and electromagnetic radiations and the results of the in vivo tests provide the substantial promise of future smart contact lenses.

INTRODUCTION

Recent advances in wearable electronics have been substantial (*1*–*4*). They show promise for continuous physiological monitoring of the human body (including the epidermis, mouth, and eyes), which generates vital physical signs and metabolites in body fluids (*5*–*11*). Especially, smart contact lenses are being extensively studied as a platform to continuously monitor the vital signs in the eyes and in tears that contain biomarkers associated with various diseases, including diabetes and glaucoma (*9*, *10*). In addition, they offer the potential for expanded applicability in other areas, such as smart devices for drug delivery and augmented reality. Obviously, the softness of these smart contact lenses is essential for the users' comfort over long periods of time (*9*, *10*, *12*). Apart from their comfort, previous results on smart contact lenses have operated intermittently in wireless ways, which can limit their continuous, long-term use, hindering the wearer's activity and therefore requiring energy storage devices. However, the rigidity, heat generation, and relatively large sizes of conventional batteries make them unsuitable for the soft, smart contact lens.

To overcome these limitations, we introduce the first approach for fabricating a soft, smart contact lens with a wirelessly rechargeable, solid-state supercapacitor that enables the continuous operation of electronic devices. An activated carbon–based, solid-state, electric double-layer supercapacitor was formed using the microscale direct ink writing (DIW) process for the soft, smart contact lens. Supercapacitors are known to exhibit long cycle lives and high-power density (*13*, *14*), which are suitable for consistent wireless charging and discharging for operating the electronic devices in the smart contact lens. In our approach, this printed supercapacitor also serves as a physical support for three-dimensional, layer-by-layer integration with the electronic circuits and antenna as its wireless charging components, which is known to be a challenging step because of the limited area of the smart contact lens. This wireless charging system is combined with the solid-state supercapacitor to enable continuous and repetitive operation of the smart contact lens with no external electrical port. The stretchable geometries of the antenna, which occupies most of the area of the smart contact lens, are formed using hybrid nanostructures of ultralong silver nanofibers (AgNFs) and fine silver nanowires (AgNWs). In addition, a stretchable hybrid substrate, which is composed of rigidly reinforced islands and a soft matrix, is used to improve the stretchable endurance of the brittle components of the device against the mechanical deformations of the contact lens. These systems exhibited superb endurance after 300 cycles with the biaxially tensile strain of 30%. The resulting smart contact lens provides both high softness and comfort without obstructing the wearer's view, and it protects the electrical devices from tear fluid over a 7-day period. In addition, the wireless charging of this smart contact lens avoided abrupt heating and maintained a stable temperature for the eye, which ensured that the wearer's eyes were safe. A human pilot trial and in vivo tests conducted using live rabbits demonstrated the biocompatibility of this lens during the charging and discharging processes.

RESULTS

Direct printing of a solid-state supercapacitor for a soft, smart contact lens

Figure 1A illustrates a schematic layout of a soft, smart contact lens where the wirelessly chargeable, solid-state supercapacitor is three-dimensionally integrated with the rectifier circuit, antenna, and light-emitting diode (LED). The upper layer of the smart contact lens includes the wireless power transfer (WPT) unit (i.e., the antenna-rectifier element), and the lower layer contains the solid-state supercapacitor, which repeatedly stores and uses electric power. In addition,

[1]Nano Science Technology Institute, Department of Materials Science and Engineering, Yonsei University, Seoul 03722, Republic of Korea. [2]Center for Nanomedicine, Institute for Basic Science (IBS), Seoul 03722, Republic of Korea. [3]Department of Energy Engineering, School of Energy and Chemical Engineering, Ulsan National Institute of Science and Technology (UNIST), Ulsan 44919, Republic of Korea. [4]Department of Materials Science and Engineering, Wearable Platform Materials Technology Center, Korea Advanced Institute of Science and Technology (KAIST), Daejeon 34141, Republic of Korea.
*These authors contributed equally to this work.
†Corresponding author. Email: jang-ung@yonsei.ac.kr (J.-U.P.); syleek@unist.ac.kr (S.-Y.L.)

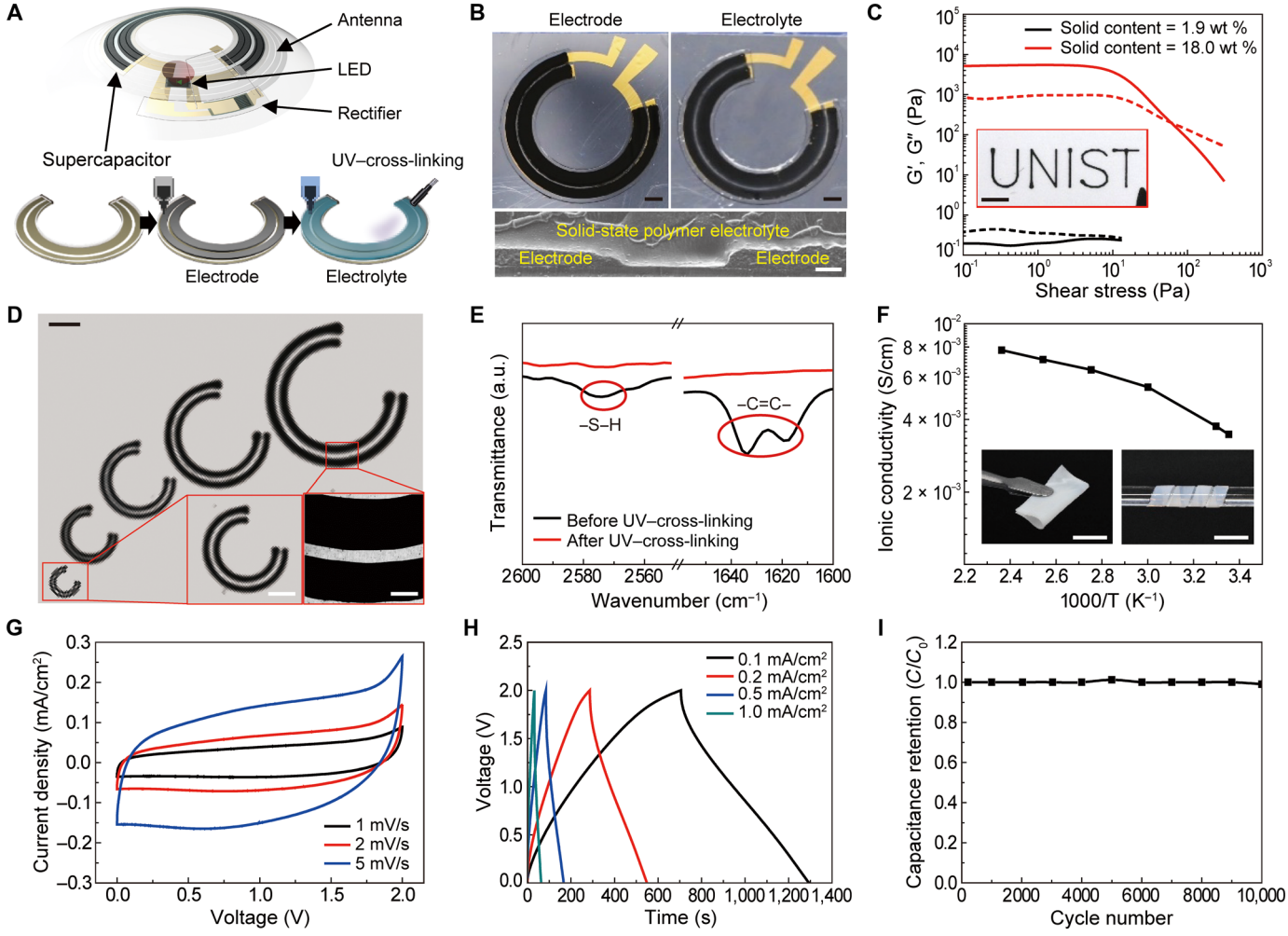

Fig. 1. DIW-based fabrication and characterization of the MIS-supercapacitor. (**A**) Schematic of the smart contact lens and DIW-based fabrication process of the monolithically integrated MIS-supercapacitor with an arc-shaped form factor. (**B**) Top-view photographs (upper images) and cross-sectional scanning electron microscopy (SEM) image (lower images) of the electrodes and solid-state polymer electrolyte of the MIS-supercapacitor (black scale bars, 1 mm; white scale bar, 50 μm). (**C**) Viscoelastic properties (G′ and G″) of the electrode inks as a function of shear stress. The inset is a photograph of a letter ("UNIST")–shaped electrode fabricated with the electrode ink (solid content, 18.0 wt %) on a polyethylene terephthalate (PET) substrate. Scale bar, 2 mm. (**D**) Photograph of in-plane electrodes with various dimensions (ranging from the micrometer to the millimeter scale) fabricated through the DIW process. The widths of electrodes varied from 100 μm to 1 mm at a fixed electrode gap of 100 μm (black scale bar, 2 mm; white scale bars, 500 μm). (**E**) Changes in the characteristic FT-IR peaks assigned to the thiol (—SH) groups (2575 cm^{-1}) and acrylic C═C bonds (1610 to 1625 cm^{-1}) in the thiol-ene polymer network skeleton before and after UV irradiation. (**F**) Ionic conductivity of the solid-state polymer electrolyte as a function of temperature (up to 150°C). The inset shows the mechanical flexibility of the solid-state polymer electrolyte. Scale bars, 1 cm. (**G**) CV curves of the MIS-supercapacitor as a function of scan rate (1, 2, and 5 mV/s). (**H**) GCD profiles at various current densities (0.1 to 1.0 mA/cm^2). (**I**) Cycling performance of the MIS-supercapacitor (measured at a constant charge/discharge current density of 3.0 mA/cm^2).

the LED is integrated as an indicator to demonstrate the wireless operation of the smart contact lens. This monolithically integrated solid-state supercapacitor (MIS-supercapacitor) has an arc-shaped form factor that is suitable for securing maximum energy density within the limited area of this contact lens (diameter, 9 mm), and it allows certain deformability under stretching of this soft lens. This smart contact lens also prevents interference with the wearer's field of vision because all of the components of the device are outside the wearer's pupil. In addition, the design of the MIS-supercapacitor includes an in-plane electrode configuration to minimize the potential for the failure of the internal short circuit during abrupt conditions (*15*).

The MIS-supercapacitor consists of carbon electrodes [activated carbon + multiwalled carbon nanotubes (MWCNTs) + polyvinylidene fluoride (PVdF) binders + polyvinylpyrrolidone (PVP) dispersant] and a solid-state polymer electrolyte (thiol-ene polymer network skeleton + ionic liquid). The arc-shaped form factor and limited area of the MIS-supercapacitor require its components (electrodes and solid-state electrolyte) to be produced by a high-precision, microscale fabrication technique. To address this issue, we used the computer-assisted, DIW technique. The DIW technique is known as a scalable and versatile fabrication method that can produce objects with arbitrary shapes with high precision without the need for expensive tools, complicated processing steps, and masks (*16*). The DIW-based dispensing procedures of the electrode ink and the electrolyte ink are displayed in movies S1 and S2, respectively. Figure 1B shows photographs (top view) and scanning electron microscopy (SEM) image (cross-sectional view) of the resulting electrodes and the solid-state

electrolyte prepared by the DIW process. The schematic layout of the printed supercapacitor is depicted in fig. S1. Note that the in-plane electrodes were built successfully on top of the gold (Au) current collector after being spatially separated by the solid-state polymer electrolyte.

The electrode ink was prepared by mixing the electrode components (activated carbon, MWCNT, PVdF, and PVP) with *N*-methyl-2-pyrrolidone (NMP), which was chosen as the processing solvent. To enable the DIW-driven microfabrication of the electrodes, the electrode ink must exhibit (i) a uniform dispersion of the activated carbon and MWCNT and (ii) rheological characteristics (specifically, thixotropic fluid behavior) that are tailored for the DIW process. The PVP additive, which is known to be an effective dispersant for carbon materials in an organic solvent, enabled the good dispersion state of the activated carbon and MWCNT (fig. S2A) in the electrode, thereby achieving stable dispensing through the micronozzle (diameter, 100 μm) (fig. S2B) (*17*, *18*). In addition, the well-dispersed electrode ink contributed to the higher electrical conductivity of the resulting electrode (fig. S3). The rheological analysis of the electrode ink [solid content, 18.0 weight percent (wt %), i.e., mass fraction of the activated carbon/MWCNT] provided high apparent viscosity (≈127 Pa·s at a shear rate of 1.0 s^{-1}), and the viscosity tended to decrease as the shear rate increased (fig. S4). In addition, the electrode ink exhibited a thixotropic fluid behavior (specifically, crossover of G′ and G″ with shear stress) (Fig. 1C), which was a prerequisite condition for the DIW process (*19*). The ink, which had a thixotropic fluid behavior, was dispensed through the micronozzle under shear stress, and the dispensed ink showed solid-like behavior in the absence of shear stress. Such well-tailored rheological properties of the electrode ink enabled the successful fabrication of a letter ("UNIST")–shaped electrode using the DIW process (inset of Fig. 1C). In comparison, the low solid content (e.g., 1.9 wt %) had typical Newtonian fluid behavior with very low viscosity (0.43 Pa·s at a shear rate of 1.0 s^{-1}), so it failed to form a solid-like shape during the DIW process (fig. S5A). In addition, when we increased the solid content (to 25.0 wt %), the corresponding electrode ink caused a nozzle-clogging problem (fig. S5B). Figure 1D shows that the optimized electrode ink (solid content, 18.0 wt %) enabled the fabrication of the electrodes with various dimensions ranging from the micrometer to the millimeter scale. Specifically, the widths of the resulting electrodes with the in-plane configuration varied from 100 μm to 1 mm at a fixed electrode gap of 100 μm, exhibiting the scalability and high resolution of the electrodes fabricated using the DIW process.

To achieve reliable use of a power source in the smart contact lens without safety concerns, a solid-state electrolyte is highly preferred in the power source instead of conventional liquid electrolytes. Thus, we designed a new solid-state polymer electrolyte with stable electrochemical performance and flexibility. This electrolyte consisted of an ionic liquid that acts as an ion-conducting medium and a thiol-ene polymer network skeleton. The electrolyte ink was prepared by mixing an ionic liquid [1-ethyl-3-methylimidazolium bis(trifluoromethylsulfonyl)imide ([EMIM][TFSI])] with ultraviolet (UV)–cross-linkable thiol-ene monomers [trimethylolpropane tris(3-mercaptopropionate (TMPPT; thiol monomer)/trimethylol propanetriacrylate (TMPTA; ene monomer) = 1/2 (mol/mol)], in which the composition ratio of the [EMIM][TFSI]/thiol-ene monomers was 85/15 (w/w). The [EMIM][TFSI] ionic liquid is known to provide high ionic conductivity and a thermal safety feature (*20*). The thiol-ene monomers were chosen because of "click reaction"–based facile synthesis/versatile chemistry and exceptional mechanical flexibility of the resulting polymers (*21*–*23*).

The electrolyte ink was dispensed directly on top of the previously fabricated electrodes and uniformly covered the entire arc-shaped area (movie S2). Subsequently, the electrolyte ink was subjected to the UV-assisted click reaction of the thiol-ene monomers in the presence of the [EMIM][TFSI] ionic liquid, resulting in the self-standing, solid-state polymer electrolyte. The synthesis of the thiol-ene polymer network skeleton was verified by observing the change in the characteristic Fourier transform infrared (FT-IR) spectroscopy peaks assigned to the thiol groups (—S—H) (2575 cm^{-1}) (*24*, *25*), and the acrylic C═C bonds (1610 to 1625 cm^{-1}) before and after the UV irradiation (Fig. 1E) (*26*, *27*). In addition, the gel content {i.e., insoluble polymer fraction after solvent [dimethyl carbonate (DMC) followed by acetone] extraction} of the resulting thiol-ene polymer network skeleton was estimated to be higher than 99 wt %, verifying that the curing of the thiol-ene monomers was completed by the UV irradiation (*28*, *29*). The resulting solid-state polymer electrolyte showed high ionic conductivity (~10^{-2} S/cm at room temperature) (Fig. 1F) and good electrochemical stability up to 3.5 V (versus Pt/Pt^{2+}) (fig. S6). In addition, the solid-state polymer electrolyte was folded and wound along the rod (diameter, 5 mm) (inset of Fig. 1F), exhibiting good mechanical flexibility without concern that the electrolyte could leak. The dimensional integrity and ionic conductivity of the solid-state polymer electrolyte were stable at a high temperature, i.e., 150°C (fig. S7). The solid-state polymer electrolyte was also compatible with the vapor deposition of the packaging material on the MIS-supercapacitor (fig. S8). These results demonstrated that the solid-state polymer electrolyte was structurally and dimensionally stable under harsh operating conditions.

On the basis of the understanding of the electrodes, the solid-state polymer electrolyte, and the DIW process described above, we printed the arc-shaped MIS-supercapacitor directly for a soft, smart contact lens, in which a parylene-based packaging layer was introduced to prevent potential leakage of the supercapacitor components to the eyes. Figure 1G shows the cyclic voltammetry (CV) curves of the MIS-supercapacitor as a function of scan rate. Normal capacitive charge/discharge behaviors were observed, and they appeared to be similar to those of conventional electric double-layer capacitors. In addition, the MIS-supercapacitor showed normal galvanostatic charge/discharge (GCD) profiles at various current densities (0.1 to 1.0 mA/cm^2), as shown in Fig. 1H. The symmetric charge and discharge profiles of the GCD profiles revealed an ideal capacitive characteristic. More notably, the MIS-supercapacitor showed a stable cycling performance (at a constant charge/discharge current density of 3.0 mA/cm^2) up to 10,000 cycles (Fig. 1I). This reasonable cycling performance of the MIS-supercapacitor, in collaboration with the wireless charging system, is expected to facilitate the long-term use of the integrated smart contact lens. To the best of our knowledge, this is the first report on power source–integrated smart contact lens with sustainable electrochemical performance.

WPT system

The wireless functionalities are essential to improve the convenience of wearable electronics. Figure 1 shows the solid-state supercapacitor as an energy storage device that can be miniaturized to fit onto the lens. The WPT circuit was fabricated for charging this supercapacitor wirelessly, as shown in Fig. 2A. This WPT unit was composed of the stretchable antenna and rectifier where ultrathin diodes and capacitors

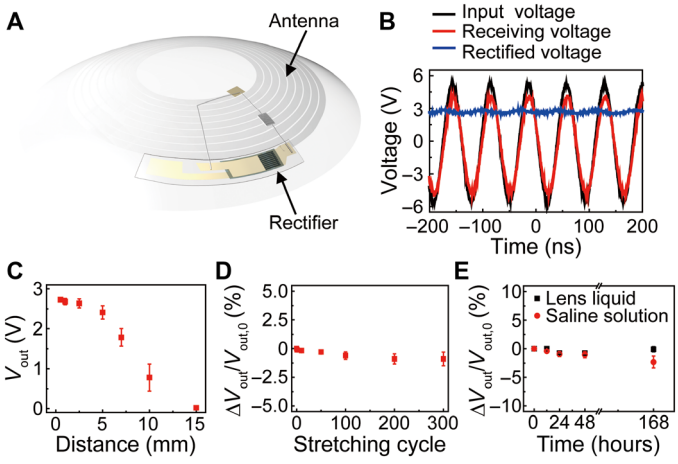

Fig. 2. Characteristics of the WPT system. (**A**) Schematic image of the WPT circuit composed of AgNF-AgNW–based antenna and rectifier. (**B**) Rectified properties of the fabricated circuit. (**C**) Distribution of rectified voltage according to the transmission distance (from 1 to 15 mm). **(D)** Relative change in rectified voltage as a function of stretching-releasing cycles (biaxially tensile strain of 30%). (**E**) Relative change in rectified voltage after immersion tests using lens liquid and saline solution. Each data point indicates the average for 50 samples, and error bars represent the SD.

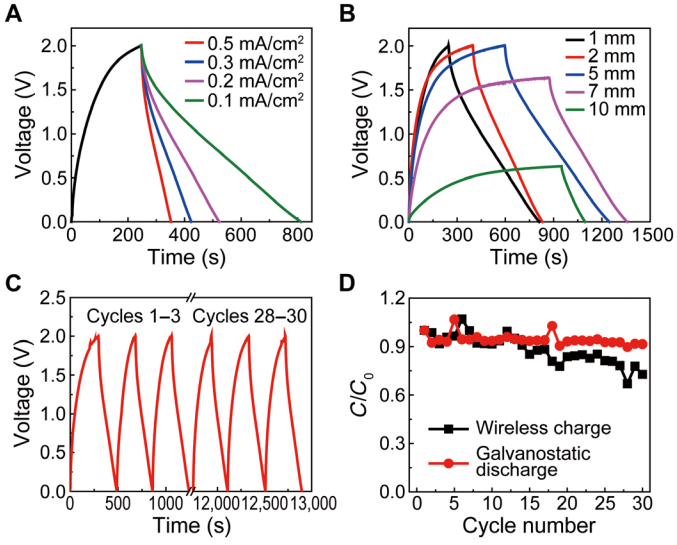

Fig. 3. Wireless charging system. (**A**) Characteristics of wireless charging/discharging by current densities. (**B**) Wireless charging/discharging profiles according to the transmission distance (from 1 to 10 mm). (**C**) Cyclic performances of the wireless charging system. (**D**) Capacity retention by the cyclic numbers.

are integrated. This rectifier was embedded inside the rigidly reinforced region of the hybrid layer and located outside the pupil to avoid interfering with the wearer's vision. The detailed processing is described in Materials and Methods. Hybrid networks of ultralong AgNFs and AgNWs were used as the stretchable antenna. The electrospun AgNFs formed continuous networks as the main conductive paths, and the fine AgNWs partially filled the vacant areas between the AgNFs. The average diameters of AgNF and AgNW were 432 ± 35 and 20 ± 5 nm, respectively. Sheet resistance (R_s) and transmittance of this transparent AgNF-AgNW hybrid networks were controlled by the electrospinning time of AgNFs. R_s and transmittance of the hybrid decreased as the electrospinning time increased. Figure S9 plots the transmittance (wavelength, 550 nm) and R_s values of the AgNF-AgNW hybrid films as a function of the area fraction of AgNF. The AgNWs bridged across individual AgNFs, forming conductive paths to preserve the resistance of these narrow antenna patterns (width, 300 μm). As a transparent antenna for the WPT system, the AgNF-AgNW hybrid films had an R_s of 0.31 ± 0.05 ohm per square, with a transparency of 72% (wavelength, 550 nm). The design of the antenna for WPT is described in fig. S10A. In addition, the resonance properties of the antenna are also described in fig. S10B. As plotted in fig. S10B, the fabricated antenna (connected with a capacitor of 180 pF) has the resonance frequency of 13.56 MHz. Figure 2B shows the rectifying characteristics of the WPT unit. In this wireless circuit, power reception was achieved inductively by the antenna (black and red lines in Fig. 2B). The power signal that was received wirelessly as an alternating current (AC) (red line in Fig. 2B) was converted into a direct current (DC) (blue line in Fig. 2B) in the rectifier for storing energy in the supercapacitor. The rectifier was composed of the p-type/intrinsic/n-type (PIN) diodes fabricated using an ultrathin Si nanomembrane (thickness, 200 nm) and SiO_2-based capacitor (fig. S11). The DC signal converted using this rectifier exhibited a bias of 2.8 root mean square voltage (V_{rms}), with an input AC signal of 3.3 V_{rms}. This wireless power transmission is also dependent on the distance between the antennas, and Fig. 2C shows the distribution of the output signal (or rectified voltage) according to this distance. The antenna in this circuit had a diameter of 1.1 cm, and the rectified voltage could be reliably preserved for a distance less than ~5 mm (*30*).

For a soft, smart contact lens, this WPT circuit must have good mechanical stretchability and chemical stability to endure various types of stimulations (e.g., deformation during wearing or tear exposure). In this circuit, the antenna was composed of stretchable AgNF-AgNW hybrid conductors, and the rigid rectifier circuit was embedded inside the mechanically reinforced region of the rigid soft hybrid layer (*10*, *30*–*32*). Therefore, the circuit had negligible degradation in its electrical performance even during the stretching state (30% in biaxially tensile strain), as shown in fig. S12. This biaxial stretchability is suitable for a soft contact lens that needs to be turned inside out. The endurance test against its repetitive cyclic stretching to the biaxially tensile strain of 30% was performed (Fig. 2D). Figure 2D shows that the output voltage of the WPT circuit exhibited negligible change, even after 300 cycles of stretching and releasing, with the biaxially tensile strain of 30%. In addition, this circuit was passivated by depositing a parylene layer (thickness, 500 nm) before it was embedded inside a soft contact lens, and it showed almost constant output voltages even after being stored for 168 hours in saline solution and the liquid for lens cleaning (Fig. 2E).

Wireless charging system

Using the miniaturized supercapacitor in Fig. 1 and the WPT system in Fig. 2, we conducted the wireless charging/galvanostatic discharging of the supercapacitor. For this characterization, these supercapacitor and WPT circuit (antenna-rectifier) were interconnected in series. Figure 3A shows the profiles of the wireless charging/galvanostatic discharging with a transmission distance of 1 mm between the antennas. The supercapacitor was fully charged during the wireless charging conditions (fully charged voltage, 1.8 V), similar to a wired manner. As shown in Fig. 3A, this supercapacitor was charged completely in a relatively short time (~240 s). In addition, the current density in the wireless charging state was expected to be

~0.2 mA/cm^2, compared with Fig. 1H and the discharging curves in the wireless charging/galvanostatic discharging profiles. Figure 3B exhibits the dependence of this wireless charging/galvanostatic discharging characteristic on the transmission distance (from 1 to 10 mm), and this wireless charging/discharging performance was negligibly degraded when the distance was less than ~5 mm. When the distance increased above this threshold, the supercapacitor did not reach the completely charged voltage (pink and green lines in Fig. 3B). In addition, the cyclic repetition of this wireless charging/discharging behavior was tested, and no notable change was observed even after 30 cycles, as plotted in Fig. 3C. In addition, Fig. 3D shows that the capacity retention after 30 cycles was over 90%. These results indicated that this wirelessly rechargeable supercapacitor system can provide reliable performance, which suggests a substantial potential for its long-term use for smart contact lenses.

Fully integrated soft, smart contact lens system

Figure 4 shows the characteristics of a wirelessly rechargeable soft, smart contact lens where the supercapacitor, antenna, rectifier circuit, and LED are fully integrated with a stretchable form. Figure 4A illustrates the schematic layout of this contact lens, and Fig. 4B shows a photograph of the lens. The antenna-rectifier circuit was placed in the upper layer, and the supercapacitor was located in the lower layer. After integrating these two layers, all electronic components were encapsulated by a silicone elastomer, a commercially available soft contact lens material, and then successively molded into the shape

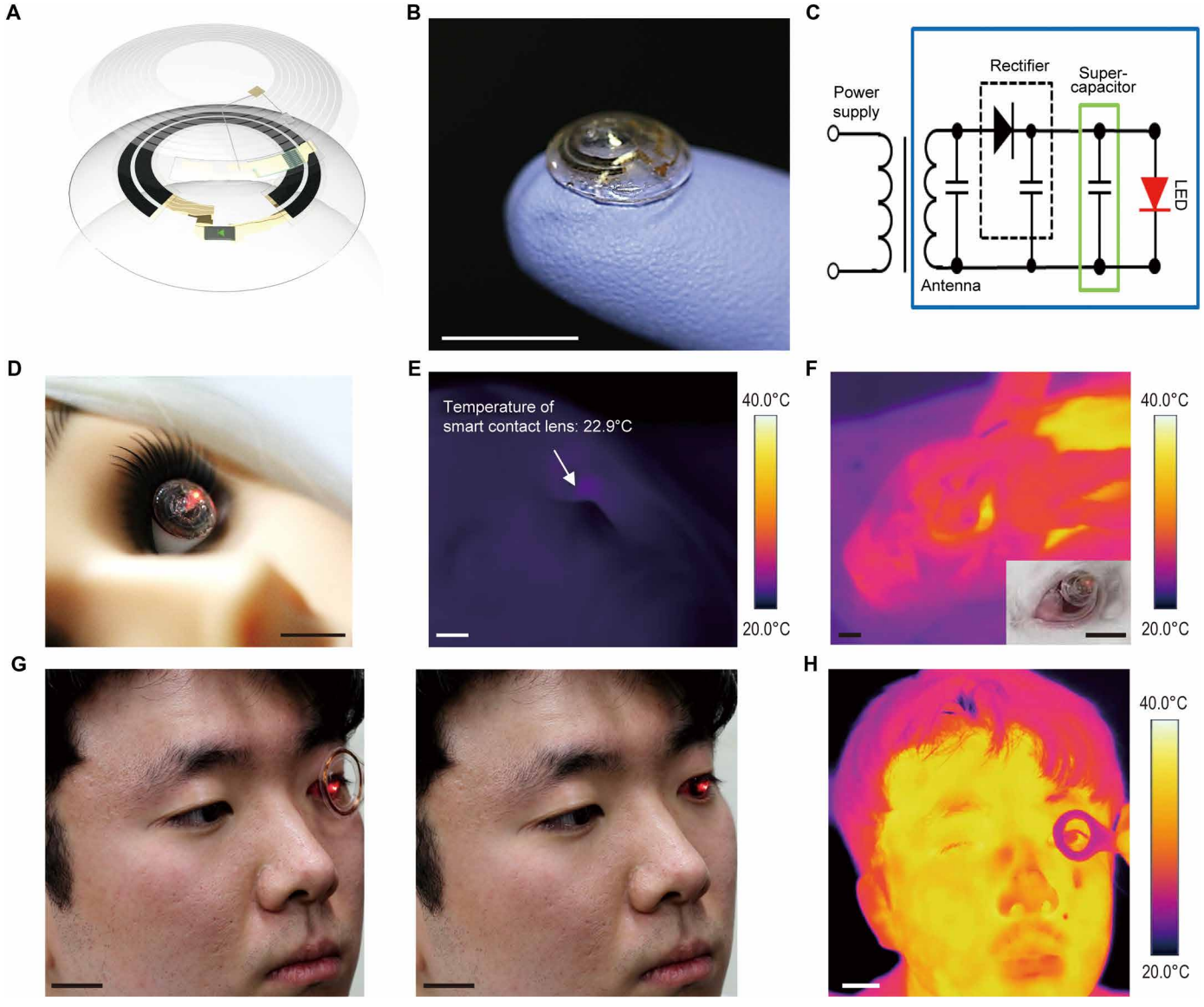

Fig. 4. Fully integrated soft, smart contact lens system. (**A**) Exploded illustration of the fully integrated soft, smart contact lens. (**B**) Photograph of the fully integrated soft, smart contact lens. Scale bar, 1 cm. (**C**) Circuit diagram of the fully integrated soft, smart contact lens. (**D**) Photograph of the soft, smart contact lens on an eye of a mannequin. Scale bar, 1 cm. (**E**) IR image of the soft, smart contact lens on an eye of a mannequin. Scale bar, 1 cm. (**F**) IR image and photograph (inset) during the discharging state on the eye of a live rabbit eye. Scale bars, 1 cm. (**G**) Photographs of a person wearing the operating soft, smart contact lens (left, charging state; right, discharging state with LED on-state). Scale bars, 2 cm. (**H**) Heat tests while a person is wearing the operating soft, smart contact lens. Scale bar, 2 cm. Photo credits: (B and D to F) Jihun Park, Yonsei University; (G and H) Joohee Kim, Yonsei University.

of a contact lens. The fabrication processing steps of this contact lens is depicted in fig. S13. When this smart contact lens was driven wirelessly, the integrated LED indicated the status of wireless charging and discharging. The circuit diagram of this soft, smart contact lens is exhibited in Fig. 4C. For example, the wireless charging of the supercapacitor using the WPT system (the antenna and rectifier) could turn on the LED pixel. As its first test, this smart lens was operated on an eye of a mannequin, and Fig. 4D presents the LED light emission from this contact lens in the discharged state. As shown in the inset of movie S3, wireless charging of this supercapacitor (for 45 s) operated the LED pixel continuously (over 60 s) in the "on" state. In addition, during the wireless operation of this lens, the generation of heat was monitored using an infrared (IR) camera (Fig. 4E and movie S3). The temperature of this lens was maintained at ~22.9°C without any significant generation of heat during the charging or discharging states, and this temperature was close to the temperature of the surroundings. Although the WPT from the transmitting coil to the lens increased the temperature of this coil to ~38.8°C, which was slightly higher than the temperature of the surroundings, its wireless function prevented this coil from touching the eye or the contact lens. According to the simulation results for specific absorption rate (SAR) for a person, the maximum SAR of this soft, smart contact lens system was calculated as ~0.9 W/kg (fig. S14), which is much lower than the regulation value of SAR (10 W/kg) (*33*). These results indicated the reliability of this soft, smart contact lens against thermal or electromagnetic field radiation. For an in vivo test, this contact lens was also worn on an eye of a live rabbit. Figure 4F indicates its reliable operation with no noticeable adverse effects and no abrupt generation of heat (with maintaining its temperature at ~37°C). As a human pilot trial, Fig. 4G and movie S4 show a human eye wearing this smart contact lens, which allowed testing all of its functions, including the wireless charging/discharging of the supercapacitor and the operation of the LED. Figure 4H and movie S4 also indicate negligible fluctuation of heat during its wireless operation, and no overt reaction of the human cornea to this lens was observed.

DISCUSSION

The soft, smart contact lens reported here could charge a supercapacitor wirelessly for continuous operations of electronic devices. In this research, electronic components, including a stretchable antenna, rectifier circuits, LEDs, and a supercapacitor, were fully integrated as a soft, smart contact lens without obstructing the wearer's view, which enabled continuous and reliable wireless charging and discharging processes. In addition, various stability tests (thermal, cyclic, and immersion tests) demonstrated the long-term usability of this soft, smart contact lens. Furthermore, the human pilot trial and in vivo studies conducted using live rabbits demonstrated its good biocompatibility, which allows it to be used as a platform for the miniaturized, wearable electronics with continuous operation.

MATERIALS AND METHODS

Preparation of electrode and electrolyte inks for the DIW process

The electrode ink for the DIW process was prepared by mixing activated carbon (MSP, Kansai Coke and Chemicals) with MWCNT (NC3100, Nanocyl) and PVdF binder in NMP, in which the composition ratio of AC/MWCNT/PVdF was 85/10/5 (w/w/w), and 1.1 wt % PVP was added as a dispersant. To prepare the electrolyte ink, an ionic liquid [EMIM][TFSI] was mixed with the UV-curable thiol-ene monomers, TMPPT and TMPTA [TMPPT/TMPTA, 1/2 (mol/mol)], incorporating 1.0 wt % 2,2-dimethoxy-2-phenylacetophenone as a photoinitiator. The composition ratio of the [EMIM][TFSI]/thiol-ene monomers was 85/15 (w/w).

Fabrication of MIS-supercapacitors

The electrode and electrolyte inks were printed using a computer-assisted DIW process based on a multifunctional printing system (Enjet Inc., South Korea). The electrode and electrolyte inks were loaded into a 1-ml plastic syringe, and then the ink-containing syringe was equipped to the printing apparatus. The typical printing speed and flow rate for the electrode and electrolyte inks were 1 mm/s at 1 μl/min and 2 mm/s at 3 μl/min, respectively. The letter ("UNIST")–shaped electrodes and the arc-shaped electrodes with various dimensions were fabricated on PET film substrates. To fabricate the MIS-supercapacitor electrodes, the electrode ink was printed on top of the patterned Cr/Au metal electrode of the smart contact lens substrate. Then, the printed electrodes were dried at 120°C for 12 hours in a vacuum oven. Subsequently, the electrolyte ink was dispensed directly on top of the previously fabricated electrodes and consecutively subjected to UV irradiation (Hg UV-lamp; irradiation peak intensity, 2000 mW/cm^2; Lichtzen), yielding a UV–cross-linked solid-state polymer electrolyte. Last, the resulting electrode/electrolyte assembly was conformally sealed with parylene C coating (thickness, 500 nm) by a vapor deposition process.

Preparation of the rectifier

The process began by defining p- and n-doped regions on silicon-on-insulator (SOI) wafer (Soitec, unibond with 200-nm top p-type Si layer with resistivity of 14 to 22 ohms·cm, and 400-nm-thick buried oxide layer) via impurity diffusion. Boron was predeposited in the furnace at the temperature of 1050°C for 70 s under the flow of N_2 (1000 sccm) using the rapid thermal annealing (RTA) process to diffuse the boron concentration uniformly across the 200-nm-thick top silicon wafer. After photolithographically patterning the SiO_2 (thickness, 300 nm) deposited by plasma-enhanced chemical vapor deposition (PECVD) on the p-doped area, phosphorus was deposited in the RTA furnace at 1050°C for 120 s under the flow of N_2 (1000 sccm) in order to convert p-type into n-type. Subsequently, the SiO_2 and SiO_x on the surface were removed using buffered hydrofluoric acid (HF) solution. The silicon p-n diode on the SOI wafer was transferred onto the target substrate system (500-nm-thick parylene/800-nm-thick Cu film/Si wafer) by etching away the buried oxide layer of the SOI wafer with 50% HF solution, and then picking up the Si diode with PDMS (polydimethylsiloxane) stamp. After transfer, the anode and cathode (Cr/Au, 3/100 nm) of the diode were deposited and patterned photolithographically. After that, the capacitor for the rectifier was manufactured. In the capacitor, the bottom electrode was connected to the cathode (n-type side of the diode), and the 300-nm-thick SiO_2, dielectric material for capacitance, was deposited by PECVD. The top electrode of the capacitor (Cr/Au, 3/200 nm) was also deposited and patterned.

Fabrication of the WPT system

To assemble the stretchable and transparent antenna for WPT, the AgNFs were electrospun on the sample where the rectifier circuit was manufactured. Subsequently, the AgNWs were also electrosprayed

on the sample. Then, the hybrid films of AgNF-AgNW were patterned by photolithography and the wet etching process. After that, the capacitor (180 pF) was connected to match the resonance frequency (13.56 MHz).

Embedding of the hybrid substrate or the integrated circuit in the contact lens

For the embedded structures, the fabricated circuit was placed within the mold for the contact lens. Subsequently, the contact lens material (elastofilcon A, E_{LENS} = ~0.09 MPa) was fulfilled and thermally cured at 100°C for 1 hour, with pressure of 313 kPa. After curing, the integrated circuit embedded in the contact lens was detached from the mold.

Electrical characterization

The four-point probe method was used for the measurement of sheet resistance using a probe station with a Keithley 4200-SCS semiconductor parametric analyzer. The electrical characteristics of the Si diodes and real-time sensing of the glucose sensor were conducted using a probe station (Keithley 4200-SCS). The *I*-*V* curves of the Si diodes were measured with the bias from −5 to 5 V.

Characterization of MIS-supercapacitors

The dispersion state of the printed electrodes in the MIS-supercapacitors and the cross-sectional structure of the MIS-supercapacitors were examined by SEM (S-4800, Hitachi). The electrical conductivities of the printed electrodes were estimated using a four-point probe (CMT-SR1000N, Advanced Instrument Technology) technique. The rheological properties of the printed electrode inks were measured using a rheometer (Haake MARS 3, Thermo Electron GmbH). The UV curing reaction of the printed solid-state polymer electrolyte was examined using an FT-IR spectrometer (Alpha, Bruker) with a spectral resolution of 4 cm^{-1}. The gel content of the solid-state polymer electrolyte was estimated by measuring its weight loss after being subjected to solvent (DMC at 70°C for 8 hours and, subsequently, acetone at room temperature for 24 hours) extraction. The ionic conductivity of the printed solid-state polymer electrolyte was characterized by the AC impedance over the frequency range from 10^{-3} to 10^{6} Hz in a temperature range of 25 to 150°C. The electrochemical stability window of the printed solid-state polymer electrolyte was measured via linear sweep voltammetry (LSV) analysis performed using a symmetric cell (Pt | electrolyte | Pt) at a scan rate of 1.0 mV/s. The printed solid-state polymer electrolyte was wound around a cylindrical glass rod (diameter, 5 mm) to examine its mechanical deformability. The cell performance of the MIS-supercapacitor was measured using a potentiostat/galvanostat (VSP classic, Bio-Logic) at various charge/discharge conditions.

Wireless measurements and operations

For wireless operations of wireless display and soft, smart contact lens, the power was generated and wirelessly transmitted by the waveform generator (Keysight 33520B). The transmitted waveform was measured by the oscilloscope (Keysight MSOX3032T).

Thermal characterization

For the thermal characterization during in vivo test, the temperature was measured by an LWIR camera (T650sc, FLIR Systems, Wilsonille, OR, USA). The temperature distribution of the images and video was analyzed using the FLIR ResearchIR software (Research IR Max, FLIR Systems).

SAR simulation

The finite-element analysis was conducted to simulate the maximum SAR for a person. The simulations were performed using the commercial software Ansoft HFSS. In the simulation, the antenna was located under the human head model, and the transmitting power from the transmitter or the smartphone was set as 10 W for the extreme environment test.

Rabbit experiments

All in vivo studies were conducted according to the guidelines of the National Institutes of Health for the care and use of laboratory animals and with the approval of the Institute of Animal Care and Use Committee of Ulsan National Institute of Science and Technology (UNIST; UNISTIACUC-16-19). The Institute of Animal Care and Use Committee of UNIST was the ethics review committee. For the in vivo experiments, a male New Zealand white rabbit was used.

Human study

The protocol for this part of the study was approved by the Institutional Review Board of UNIST (UNISTIRB-18-17-A). A volunteer tested the smart contact lens, which was worn for 10 min. The smart contact lens was rinsed with contact lenses cleansing solution, followed by phosphate-buffered saline for 1 min before wearing.

SUPPLEMENTARY MATERIALS

Supplementary material for this article is available at http://advances.sciencemag.org/cgi/content/full/5/12/eaay0764/DC1

Fig. S1. The schematic layout of the printed supercapacitor.
Fig. S2. Effect of PVP additive on electrode inks.
Fig. S3. Effect of PVP additive on electrical conductivity of the resulting electrodes (without PVP additive versus with PVP additive).
Fig. S4. Viscosity of the electrode inks (solid content, 1.9 and 18.0 wt %) as a function of shear rate.
Fig. S5. Effect of solid content on electrode fabrication through DIW process.
Fig. S6. LSV profiles of the solid-state polymer electrolyte (scan rate, 1.0 mV/s).
Fig. S7. Weight retention and ionic conductivity of the solid-state polymer electrolyte at 150°C as a function of time.
Fig. S8. Weight retention and ionic conductivity of the solid-state polymer electrolyte in a vacuum as a function of time.
Fig. S9. Optical and electrical characteristics of AgNF-AgNW hybrid films.
Fig. S10. Design and properties of the antenna for WPT.
Fig. S11. Rectifier circuit based on Si PIN diodes and SiO_2-based capacitor.
Fig. S12. Biaxially stretching tests of AgNF-AgNW hybrid films.
Fig. S13. Fabrication of a fully integrated soft, smart contact lens system.
Fig. S14. SAR simulation results.
Movie S1. Video clip showing the DIW-based dispensing procedure of the electrode ink on the smart contact lens substrate.
Movie S2. Video clip showing the DIW-based dispensing procedure of the electrolyte ink on top of the previously fabricated electrodes.
Movie S3. Video clip showing wireless the charging and discharging operation on the mannequin eye.
Movie S4. Video clip showing the heat generation test in the wearing of the soft, smart contact lens on the human eye.

REFERENCES AND NOTES

1. S. Xu, Y. Zhang, L. Jia, K. E. Mathewson, K. I. Jang, J. Kim, H. Fu, X. Huang, P. Chava, R. Wang, S. Bhole, L. Wang, Y. J. Na, Y. Guan, M. Flavin, Z. Han, Y. Huang, J. A. Rogers, Soft microfluidic assemblies of sensors, circuits and radios for the skin. *Science* **344**, 70–74 (2014).
2. K. Sim, Z. Rao, H.-J. Kim, A. Thukral, H. Shim, C. Yu, Fully rubbery integrated electronics from high effective mobility intrinsically stretchable semiconductors. *Sci. Adv.* **5**, eaav5749 (2019).
3. T.-i. Kim, J. G. McCall, Y. H. Jung, X. Huang, E. R. Siuda, Y. Li, J. Song, Y. M. Song, H. A. Pao, R.-H. Kim, C. Lu, S. D. Lee, I.-S. Song, G. Shin, R. al-Hasani, S. Kim, M. P. Tan, Y. Huang, F. G. Omenetto, J. A. Rogers, M. R. Bruchas, Injectable, cellular-scale optoelectronics with applications for wireless optogenetics. *Science* **340**, 211–216 (2013).

4. H. H. Jung, J. Song, S. Nie, H. N. Jung, M. S. Kim, J.-W. Jeong, Y. M. Song, J. Song, K.-I. Jang, Thin metallic heat sink for interfacial thermal management in biointegrated optoelectronic devices. *Adv. Mater. Technol.* **3**, 1800159 (2018).
5. X. Dai, W. Zhou, T. Gao, J. Liu, C. M. Lieber, Three-dimensional mapping and regulation of action potential propagation in nanoelectronics-innervated tissues. *Nat. Nanotechnol.* **11**, 776–782 (2016).
6. W. Gao, S. Emaminejad, H. Y. Y. Nyein, S. Challa, K. Chen, A. Peck, H. M. Fahad, H. Ota, H. Shiraki, D. Kiriya, D. H. Lien, G. A. Brooks, R. W. Davis, A. Javey, Fully integrated wearable sensor arrays for multiplexed *in situ* perspiration analysis. *Nature* **529**, 509–514 (2016).
7. C. M. Boutry, L. Beker, Y. Kaizawa, C. Vassos, H. Tran, A. C. Hinckley, R. Pfattner, S. Niu, J. Li, J. Claverie, Z. Wang, J. Chang, P. M. Fox, Z. Bao, Biodegradable and flexible arterial-pulse sensor for the wireless monitoring of blood flow. *Nat. Biomed. Eng.* **3**, 47–57 (2019).
8. D.-H. Kim, N. Lu, R. Ma, Y.-S. Kim, R.-H. Kim, S. Wang, J. Wu, S. M. Won, H. Tao, A. Islam, K. J. Yu, T. I. Kim, R. Chowdhury, M. Ying, L. Xu, M. Li, H.-J. Chung, H. Keum, M. McCormick, P. Liu, Y.-W. Zhang, F. G. Omenetto, Y. Huang, T. Coleman, J. A. Rogers, Epidermal electronics. *Science* **333**, 838–843 (2011).
9. J. Kim, K. Minji, M.-S. Lee, K. Kim, S. Ji, Y.-T. Kim, J. Park, K. Na, K.-H. Bae, H. K. Kim, F. Bien, C. Y. Lee, J.-U. Park, Wearable smart sensor systems integrated on soft contact lenses for wireless ocular diagnostics. *Nat. Commun.* **8**, 14997 (2017).
10. J. Park, J. Kim, S.-Y. Kim, W. H. Cheong, J. Jang, Y.-G. Park, K. Na, Y.-T. Kim, J. H. Heo, C. Y. Lee, J. H. Lee, F. Bien, J.-U. Park, Soft, smart contact lenses with integrations of wireless circuits, glucose sensors, and displays. *Sci. Adv.* **4**, eaap9841 (2018).
11. J. Kim, M.-S. Lee, S. Jeon, M. Kim, S. Kim, K. Kim, F. Bien, S. Y. Hong, J.-U. Park, Highly transparent and stretchable field-effect transistor sensors using graphene-nanowire hybrid nanostructures. *Adv. Mater.* **27**, 3292–3297 (2015).
12. H. Lee, S. Kim, K.-B. Kim, J.-W. Choi, Scalable fabrication of flexible thin-film batteries for smart lens applications. *Nano Energy* **53**, 225–231 (2018).
13. M. Beidaghi, Y. Gogotsi, Capacitive energy storage in micro-scale devices: Recent advances in design and fabrication of micro-supercapacitors. *Energ. Environ. Sci.* **7**, 867–884 (2014).
14. C. Shen, S. Xu, Y. Xie, M. Sanghadasa, X. Wang, L. Lin, A review of on-chip micro supercapacitors for integrated self-powering systems. *J. Microelectromechanical Syst.* **26**, 949–965 (2017).
15. D. Qi, Y. Liu, Z. Liu, L. Zhang, X. Chen, Design of architectures and materials in in-plane micro-supercapacitors: Current status and future challenges. *Adv. Mater.* **29**, 1602802 (2017).
16. Y. Zhang, C. Liu, D. Whalley, Direct-write techniques for maskless production of microelectronics: A review of current state-of-the-art technologies, in *2009 International Conference on Electronic Packaging Technology High Density Packaging* (2009), pp. 497–503.
17. L. Vaisman, H. D. Wagner, G. Marom, The role of surfactants in dispersion of carbon nanotubes. *Adv. Colloid Interface Sci.* **128–130**, 37–46 (2006).
18. T. Hasan, V. Scardaci, P. H. Tan, A. G. Rozhin, W. I. Milne, A. C. Ferrari, stabilization and "debundling" of single-wall carbon nanotube dispersions in *N*-methyl-2-pyrrolidone (NMP) by polyvinylpyrrolidone (PVP). *J. Phys. Chem. C* **111**, 12594–12602 (2007).
19. J. A. Lewis, Direct Ink Writing of 3D Functional Materials. *Adv. Funct. Mater.* **16**, 2193–2204 (2006).
20. Y.-S. Ye, J. Rick, B.-J. Hwang, Ionic liquid polymer electrolytes. *J. Mater. Chem. A* **1**, 2719–2743 (2013).
21. C. E. Hoyle, T. Y. Lee, T. Roper, Thiol–enes: Chemistry of the past with promise for the future. *J. Polym. Sci.* **42**, 5301–5338 (2004).
22. C. E. Hoyle, A. B. Lowe, C. N. Bowman, Thiol-click chemistry: a multifaceted toolbox for small molecule and polymer synthesis. *Chem. Soc. Rev.* **39**, 1355–1387 (2010).
23. S.-S. Lee, K.-H. Choi, S.-H. Kim, S.-Y. Lee, Wearable Supercapacitors Printed on Garments. *Adv. Funct. Mater.* **28**, 1705571 (2018).
24. C. F. Carlborg, T. Haraldsson, K. Öberg, M. Malkoch, W. van der Wijngaart, Beyond PDMS: Off-stoichiometry thiol–ene (OSTE) based soft lithography for rapid prototyping of microfluidic devices. *Lab Chip* **11**, 3136–3147 (2011).
25. M. Willgert, M. H. Kjell, G. Lindbergh, M. Johansson, New structural lithium battery electrolytes using thiol–ene chemistry. *Solid State Ion.* **236**, 22–29 (2013).
26. H.-J. Ha, E. H. Kil, Y. H. Kwon, J. Y. Kim, C. K. Lee, S. Y. Lee, UV-curable semi-interpenetrating polymer network-integrated, highly bendable plastic crystal composite electrolytes for shape-conformable all-solid-state lithium ion batteries. *Energy Environ. Sci.* **5**, 6491–6499 (2012).
27. K.-H. Choi, S.-J. Cho, S.-H. Kim, Y. H. Kwon, J. Y. Kim, S.-Y. Lee, Thin, Deformable, and Safety-Reinforced Plastic Crystal Polymer Electrolytes for High-Performance Flexible Lithium-Ion Batteries. *Adv. Funct. Mater.* **24**, 44–52 (2014).
28. H.-J. Ha, Y. H. Kwon, J. Y. Kim, S.-Y. Lee, A self-standing, UV-cured polymer networks-reinforced plastic crystal composite electrolyte for a lithium-ion battery. *Electrochim. Acta* **57**, 40–45 (2011).
29. S.-H. Kim, K.-H. Choi, S.-J. Cho, S. Choi, S. Park, S.-Y. Lee, Printable solid-state lithium-ion batteries: A new route toward shape-conformable power sources with aesthetic versatility for flexible electronics. *Nano Lett.* **15**, 5168–5177 (2015).
30. S. Ji, B. G. Hyun, K. Kim, S. Y. Lee, S.-H. Kim, J. Y. Kim, M. H. Song, J.-U. Park, Photo-patternable and transparent films using cellulose nanofibers for stretchable origami electronics. *NPG Asia Mater.* **8**, e299 (2016).
31. A. Romeo, Q. Liu, Z. Suo, S. P. Lacour, Elastomeric substrates with embedded stiff platforms for stretchable electronics. *Appl. Phys. Lett.* **102**, 131904 (2013).
32. M. Kim, J. Park, S. Ji, S.-H. Shin, S.-Y. Kim, Y.-C. Kim, J.-Y. Kim, J.-U. Park, Fully-integrated, bezel-less transistor arrays using reversibly foldable interconnects and stretchable origami substrates. *Nanoscale* **8**, 9504–9510 (2016).
33. *IEEE Standard for Safety Levels with Respect to Human Exposure to Radio Frequency Electromagnetic Fields, 3 kHz to 300 GHz. IEEE Std C951-2005 Revis. IEEE Std C951–1991*, 1–238 (2006).

Acknowledgments

Funding: This work was supported by the Ministry of Science & ICT (MSIT) and the Ministry of Trade, Industry and Energy (MOTIE) of Korea through the National Research Foundation (2019R1A2B5B03069358, 2016R1A5A1009926, and 2018R1A2A1A05019733), the Bio & Medical Technology Development Program (2018M3A9F1021649), the Nano Material Technology Development Program (2015M3A7B4050308 and 2016M3A7B4910635), and the Industrial Technology Innovation Program (10080577 and 10080540). Also, the authors thank the financial support by the Institute for Basic Science (IBS-R026-D1) and the Research Program (2018-22-0194) funded by Yonsei University. **Author contributions:** J.P., D.B.A., J.K., S.-Y.L., and J.-U. P. conceived the idea and designed the research. E.C. performed measurements of the lens devices. B.-S.B. contributed to the project planning. **Competing interests:** The authors declare that they have no competing interests. **Data and materials availability:** All data needed to evaluate the conclusions in the paper are present in the paper and/or the Supplementary Materials. Additional data related to this paper may be requested from the authors.

Submitted 17 May 2019
Accepted 17 September 2019
Published 6 December 2019
10.1126/sciadv.aay0764

Citation: J. Park, D. B. Ahn, J. Kim, E. Cha, B.-S. Bae, S.-Y. Lee, J.-U. Park, Printing of wirelessly rechargeable solid-state supercapacitors for soft, smart contact lenses with continuous operations. *Sci. Adv.* **5**, eaay0764 (2019).

Science Advances

Printing of wirelessly rechargeable solid-state supercapacitors for soft, smart contact lenses with continuous operations

Jihun Park, David B. Ahn, Joohee Kim, Eunkyung Cha, Byeong-Soo Bae, Sang-Young Lee and Jang-Ung Park

Sci Adv **5** (12), eaay0764.
DOI: 10.1126/sciadv.aay0764

Science Advances (ISSN 2375-2548) is published by the American Association for the Advancement of Science, 1200 New York Avenue NW, Washington, DC 20005. The title *Science Advances* is a registered trademark of AAAS.